Applied Catalysis B: Environmental 90 (2009) 497–506

Contents lists available at ScienceDirect

Applied Catalysis B: Environmental

journal homepage: www.elsevier.com/locate/apcatb

Preparation, characterization and photocatalytic activity of TiO_2 impregnated with the heteropolyacid $H_3PW_{12}O_{40}$: Photo-assisted degradation of 2-propanol in gas–solid regime

G. Marcì [a,*], E. García-López [a], L. Palmisano [a], D. Carriazo [b], C. Martín [b], V. Rives [b]

[a] "Schiavello-Grillone" Photocatalysis Group, Dipartimento di Ingegneria Chimica dei Processi e dei Materiali, Università di Palermo, Viale delle Scienze, Ed. 6, 90128 Palermo, Italy
[b] GIR-QUESCAT, Departamento de Química Inorgánica, Universidad de Salamanca, 37008 Salamanca, Spain

ARTICLE INFO

Article history:
Received 27 January 2009
Received in revised form 24 March 2009
Accepted 28 March 2009
Available online 16 April 2009

Keywords:
Polyoxometalate
2-Propanol
Heterogeneous photocatalysis
TiO_2

ABSTRACT

Both commercial and home prepared TiO_2 samples impregnated with tungstophosphoric acid ($H_3PW_{12}O_{40}$) were prepared and used for the photo-assisted degradation of 2-propanol in gas–solid regime. The characterization results evidenced a good coverage of the polyoxometalate (POM) onto the surface of both types of TiO_2 samples along with a marginal effect of the presence of ethanol or HCl during the POM impregnation step on the specific surface area, porosity, morphology, crystallinity and acidity of the samples. Propene was the main intermediate product found in 2-propanol photocatalytic degradation by using the samples containing POM as the photocatalyst, whereas propanone was mainly obtained when the photocatalyst was bare TiO_2. Acetaldehyde was also an intermediate product and its amount was always significantly smaller with respect to propanone and propene (when formed). Carbon dioxide and water were the ultimate oxidation products. The selectivity to propene has been attributed to the acidity of the POM supported samples.

1. Introduction

Photocatalysis is a field of great interest that in the last decades has been proposed mainly for the abatement of pollutants existing in gaseous or liquid streams. Due to its (photo)stability and low cost, TiO_2 has been shown to be the most used photocatalyst, offering the highest light energy conversion efficiency [1]. Recently some authors have reported the use of photocatalysts consisting in a heteropolyacid supported on TiO_2 [2] or ZrO_2 [3]. In these binary materials a synergistic effect between the two components was observed and the improvement in their performance with respect to the bare materials was ascribed to the delaying of the electron–hole recombination [4]. The heteropolyacids share photochemical characteristics with the semiconductor photocatalysts [5]; indeed, both classes of materials are constituted by d^0 transition metal and oxide ions and exhibit similar electronic characteristics (HOMO–LUMO transition for the heteropolyacids and band-gap transition for semiconductors). Due to the fact that they are very soluble in polar solvents, some heteropolyacids have been used extensively in homogeneous catalysis, since they can be activated by light in photo-assisted oxidation reactions carried out in liquid phase [6,7].

Heteropolyacids, which belong to the large family of the polyoxometalates (POMs), are very strong Brönsted acids and efficient oxidants that perform fast and reversible redox multi-eletron transformations under mild conditions; hence they can act as bifunctional catalysts used in solution as acid and oxidation catalysts [8]. They have well defined structures and properties and their size are typically a few nanometers [9]. Misono et al. reported that when POMs are used as heterogeneous catalysts the nature of the reactants determined whether the reaction occurs on the surface of the catalysts or in the bulk; in fact, they distinguished three types of heterogeneous catalysis by using POMs, i.e. (i) surface, (ii) bulk type I or pseudo-liquid and (iii) bulk type II [10]. In particular, when the reactant is a polar molecule POMs absorb it in the bulk, leading to a pseudo-liquid phase type of catalysis; for apolar molecules, however, the reaction occurs only on the surface or between surface layers of the crystal [10]. Some attempts have been made to increase the surface area of these catalysts by using as supports silica MCM 41 [11], resins [12] or polysiloxane polymers [13]. A hybrid matrix where an inorganic material, as silicon alkoxide 3-isocyanatopropyltriethoxyl-silane, is linked to the inorganic POM, was prepared for ionically conducting purposes [14]. The use of a semiconductor as support can be very interesting for photocatalytic scopes as POM acts as an electron trap [4,5] and, moreover, the transfer of electrons from POM to oxygen species present in the reaction medium should enhance the reaction kinetics, as evidenced by spectroscopic studies [15].

* Corresponding author. Tel.: +39 091 238 63737; fax: +39 091 702 5020.
E-mail address: marci@dicpm.unipa.it (G. Marcì).

0926-3373/$ – see front matter © 2009 Elsevier B.V. All rights reserved.
doi:10.1016/j.apcatb.2009.03.034

Bare TiO_2 photoactivity strongly depends on several variables as preparation method, particle size, reactive surface area and ratio between anatase and rutile phases. A way to improve the activity of a photocatalyst is to increase its specific surface area and to decrease the size of the particles, reasons for which much attention has been devoted to nanostructured TiO_2 materials [16]. Particular effort should be done to obtain an optimum POM support, in order to improve the binary photocatalysts performance. Various nanostructured TiO_2 catalysts prepared by hydrolysis of titanium tetrachloride showed a good photocatalytic activity [17], moreover neither filtration nor calcination were needed during their preparation, in order to obtain a highly efficient anatase phase.

The photocatalytic degradation of 2-propanol in the presence of both oxygen and UV light at ambient temperature has been used as a probe reaction by using TiO_2 as the photocatalyst. Propanone was reported to be the main intermediate product in the photocatalytic oxidation of 2-propanol in gas–solid regime [18–21], followed by a subsequent photo-oxidation to produce ultimately CO_2. The use of a modified TiO_2, for instance by incorporating sulfuric acid during the photocatalysts preparation, leads to a high selectivity versus the formation of isoproylether [22].

It is accepted that a good reaction to probe the acid character of a catalysts is the dehydration of 2-propanol in the gas–solid regime that gives rise to the formation of propene at ambient pressure and moderate temperature (in the range 413–598 K) [23]. The selectivity to propene or propanone strongly depends on the experimental conditions, mainly temperature and gaseous ambient phase (He, N_2, H_2, O_2) and particularly on the acidity–basicity of the solid catalyst; consequently, the catalytic degradation of 2-propanol has been proposed as a test reaction to determine acid-base properties of an oxide catalyst [24].

The aim of this work is the preparation of binary photocatalysts consisting of POM supported onto TiO_2 to study the role of the POM on the photocatalysts physico-chemical characteristics and on their photocatalytic activity and selectivity versus the intermediates species obtained during the photo-degradation of 2-propanol. Two types of commercial and home prepared TiO_2 powders were impregnated with the Keggin type heteropolyacid $H_3PW_{12}O_{40}$.

2. Experimental

2.1. Preparation and characterization of the binary solids

Titanium tetrachloride (Fluka 98%) was used as the starting material without any further purification to obtain the home prepared TiO_2. $TiCl_4$ was slowly added to distilled water (volume ratio: 1:50) at room temperature [17]. The hydrolysis reaction was highly exothermic. After ca. 1 h of continuous stirring, the resulting solution was refluxed for 24 h. After the refluxing treatment, the obtained opalescent dispersion was evacuated in a rotavapor to obtain a powder (called home prepared TiO_2 or TiO_2 hp). No calcination step was accomplished. Both commercial (Degussa P25) and home prepared TiO_2 were successively impregnated by incipient wetness with a solution of a commercial polyoxometalate, tungstophosphoric acid $H_3PW_{12}O_{40}$ (Aldrich reagent grade 99.7%), named POM in the following. The Ti:POM molar ratio was held constant at 1:0.008. The POM solution was prepared in water, ethanol (Fluka 97%) or aqueous 0.05 M HCl. The final mixture containing both the TiO_2 and POM was evaporated until dryness. An annealing treatment at 120 °C under vacuum (ca. 0.1 Torr) was eventually performed.

The powders obtained were labelled as POM, the acronym P25 (TiO_2 Degussa P25) or hp (TiO_2 home prepared), indicating the type of TiO_2 present in the binary solid catalyst and followed by the medium in which the $H_3PW_{12}O_{40}$ was dissolved to accomplish the impregnation step, i.e. H_2O, EtOH or HCl (for the POM aqueous solution H_2O was omitted).

The solid samples were characterized by X-ray diffractometry (XRD) recorded at room temperature in a Philips X-ray powder diffractometer using the Cu Kα radiation and a 2θ scan rate of $2^\circ\ min^{-1}$. Nitrogen adsorption–desorption isotherms were registered in a Gemini instrument from Micromeritics. Determination of BET specific surface area (SSA) was accomplished by using a Flowsorb 2300 (Micromeritics), scanning electron microscopy (SEM) were performed using a Philips XL30 ESEM microscope, operating at 25 kV on specimens after being coated with a layer of gold. Moreover, an electron microprobe used in an energy dispersive mode (EDX) was employed to obtain information on the atomic content of W on the samples. Raman measurements were performed on pure powdered samples packed into sample cups. Spectra were recorded by a Reinshaw in-via Raman spectrometer equipped with an integrated microscope and with a charged-coupled device (CCD) camera. A He/Ne laser operating at 632.8 nm was used as the exciting source. Diffuse reflectance spectra (DRS) were recorded in the range 250–600 nm by using a Shimadzu UV-2401 PC instrument with $BaSO_4$ as the reference sample. Infrared spectra of the samples in KBr (Aldrich) pellets were obtained with a FTIR-8400 Shimadzu spectrometer and the spectra were recorded with $4\ cm^{-1}$ resolution and 256 scans. Surface acidity was studied through FT-IR spectroscopic monitoring of pyridine (Py) adsorption in a Perkin-Elmer 16PC spectrometer coupled to a high-vacuum Pyrex system. Self-supported disks were used, outgassed in situ in a special cell (built in Pyrex with CaF_2 windows) [25] at 373 K for 2 h prior to Py adsorption. Twenty scans were taken to improve the signal-to-noise ratio at a nominal resolution of $2\ cm^{-1}$. The gas was admitted into the IR cell at room temperature and after 15 min of equilibration, the gas phase was removed by outgassing at room temperature and at 373 K, then the spectra were recorded.

2.2. Photoreactivity experiments

The photoreactor operating in gas–solid regime was a continuous Pyrex fixed bed photoreactor of cylindrical shape (diameter 58 mm, height 100 mm). A porous glass septum at the bottom of the cylinder allowed to sustain the fixed bed of the solid and to distribute the inlet gaseous mixture. The corresponding fixed bed height was ca. 1 mm. The reactivity runs were carried out with 1.5 g of photocatalyst. The gas feeding the photoreactor consisted of oxygen, 2-propanol and water. 2-Propanol and water were introduced in the oxygen stream by means of a home made infusion pump and their initial concentrations were 8×10^{-5} and 3.4×10^{-4} M (relative humidity ca. 27%), respectively. Such concentrations allowed that they instantaneously vaporized in the oxygen stream at 298 K. Water was absent during the course of some selected runs in order to study its influence on the reaction. Preliminary tests were performed with the aim of determining the suitable flow rate conditions to avoid mass transport limitations on the photoreaction and consequently the flow rate at which the runs were eventually carried out was $0.5\ cm^3\ s^{-1}$. Irradiation started only when steady-state conditions were achieved, i.e. after ca. 4 h of fluxing the reactive mixture into the photoreactor in dark conditions. The steady-state conditions were considered when the outlet concentration of 2-propanol was more than 95% of the inlet value.

The reactor was vertically positioned and illuminated from the top inside of a SOLARBOX apparatus (CO.FO.ME.GRA.) equipped with solar light simulating lamp (high pressure Xe lamp of 1500 W). A water filter was located between the lamp and the photoreactor to cut-off the infrared radiation and to maintain the temperature inside the reactor at ca. 300 K. The irradiance reaching

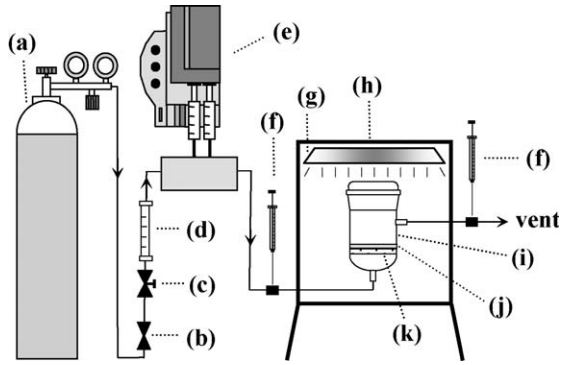

Scheme 1. Experimental set-up for the gas–solid experiments. (a) Oxygen cylinder, (b) switch valve, (c) control valve, (d) rotameter, (e) infusion pump, (f) gas-tight syringe, (g) lamp, (h) SOLARBOX, (i) photoreactor, (j) fixed bed of catalyst and (k) porous glass septum.

the photoreactor was measured by using a UVX Digital radiometer and it was equal to 1.0 mW cm^{-2} in the radiation wavelengths range between 355 and 375 nm, corresponding to an irradiance of 8.0×10^{-8} Einstein s^{-1} at 365 nm where the sensitivity of the radiometer is maximum. Scheme 1 illustrates the photoreactor and the irradiation experimental set-up.

The runs lasted ca. 6 h and samples of the reacting fluid were analysed during the course of the reaction by withdrawing 200 μl of gas from the outlet of the photoreactor by means of a gas-tight syringe. Substrate and intermediate products concentrations were measured by a GC-17A Shimadzu gas chromatograph equipped with a HP-1 column and a FID, whereas carbon dioxide was analyzed by a 60/80 Carboxen 1000 column in an HP6890 gas chromatograph equipped with a TCD.

3. Results and discussion

3.1. Physico-chemical characterization of the solids

The diffractograms of the home prepared TiO_2 samples (not shown for the sake of brevity) indicate the presence of anatase and rutile phases. The size of the crystallites, estimated by means of the Scherrer equation, were in the range 10–20 nm for anatase and 5–8 nm for rutile. No significant differences were observed by studying the same home prepared TiO_2 sample impregnated with POM either in H_2O, HCl or EtOH, even after the vacuum-annealing treatment. Also the samples obtained by impregnation of TiO_2 Degussa P25 showed X-ray diffractograms very similar to that obtained for the bare commercial TiO_2. No separate POM related peaks were revealed whichever the impregnation medium used, indicating, in any case, a homogeneous dispersion of POM onto the titanium dioxide surface with dimension of the crystalline POM tertiary structures [6] lower than the detection limit of the instrument. It is worth noting that no significant peak position or broadening of the TiO_2 peaks occurred in any case after deposition of the POM on the TiO_2 suggesting that the POM species can be positioned onto the TiO_2 surface excluding their localization in interstitial sites or substitutional positions.

The experimental values of the specific surface areas of all samples based on home prepared TiO_2 are in the range 49–51 $m^2 g^{-1}$ whereas those of the samples based on TiO_2 Degussa P25 showed surface areas in the range 38–45 $m^2 g^{-1}$. The specific surface areas of all the samples containing the POM are slightly lower on respect to the bare TiO_2 (values reported in Table 1). This slight decrease can be attributed to the coverage of the TiO_2 surface with the tungstophosphoric acid molecules suggesting that the POM units are dispersed onto the TiO_2 surface. All the nitrogen adsorption–desorption isotherms can be included into the II-type according to the IUPAC classification (see Fig. 1), which are generally associated to non-porous or macroporous materials [26]. It is worth noting that the incorporation of the POM either on TiO_2 hp and Degussa P25 does not produce appreciable changes in the shape of these isotherms, supporting again the good dispersion of the POM moieties over these oxides.

SEM observations revealed that all the samples consisted of aggregates of particles. Fig. 2 shows some representative micrographs obtained for bare and POM loaded home prepared TiO_2 samples. From Fig. 2 appears that the loading with POM increases the size of the secondary particles but does not modify their morphology. Direct and accurate measurements carried out on the SEM microphotographs allow to conclude that the loaded samples show aggregates of crystallites (secondary particles) whose size ranged between 50 and 235 nm, whereas for the bare TiO_2 hp the sizes were in the range 50–80 nm.

The same behaviour was observed for the samples obtained loading on TiO_2 Degussa P25. The SEM microphotographs are showed in Fig. 3. As far as the size of the aggregates is concerned, whichever methodology of preparation was followed, the samples based on TiO_2 Degussa P25 showed particles whose size was generally bigger than that of the corresponding sample based on the home prepared TiO_2, and it ranged between 70 and 235 nm. Moreover, in any case, when the impregnation was carried out in the presence of HCl, some larger particles appeared in the samples. The particles sizes of the various samples as determined by considering the apparent secondary particles constituting the aggregates, are reported in Table 1.

EDX measurements confirmed a homogeneous distribution of the POM onto the surface of the TiO_2 support. As reported in Table 1, the amount of tungsten measured by EDX was slightly higher than the nominal one (12–13% atoms of W on respect to the total amount of Ti + W, instead of the nominal value corresponding to 8.8%), indicating that almost all the POM was deposited onto the TiO_2 surface. EDX analyses showed also that the amount of chloride ions present both in bare and in loaded home prepared TiO_2 samples, including also those prepared in the presence of HCl, was always less than 0.2%.

The diffuse reflectance spectra of the samples (not showed for the sake of brevity) are quite similar each other showing the typical

Table 1
Specific surface areas (SSA), apparent secondary particles size, W and Ti atomic percentage and Brönsted/Lewis ratio of samples prepared by various routes.

Sample	SSA [$m^2 g^{-1}$]	SEM particle size [nm]	EDX W atomic [%]	EDX Ti atomic [%]	BPy/LPy
POM/P25	38	120–160	13.5	86.5	2.35
POM/P25–HCl	40	125–235	12.1	87.9	2.05
POM/P25–EtOH	42	70–200	12.5	87.5	n.d.
POM/hp	50	70–150	13.0	87.0	2.24
POM/hp–HCl	49	80–235	12.5	87.5	n.d.
POM/hp–EtOH	50	50–150	13.5	86.5	1.98
TiO_2 Degussa P25	45	50–100	–	–	–
TiO_2 hp	51	50–80	–	–	–

n.d., not determined.

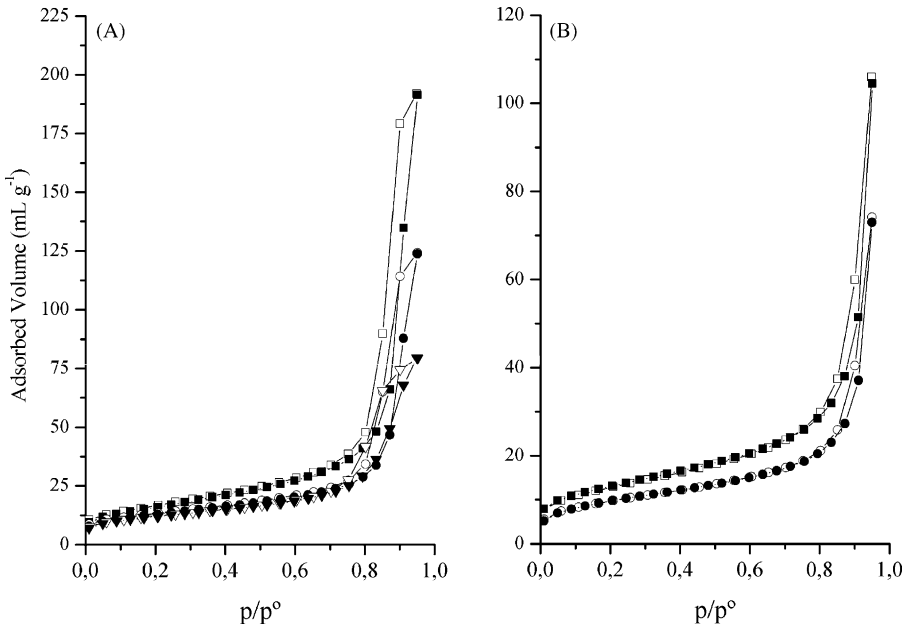

Fig. 1. Nitrogen adsorption–desorption isotherms (filled symbols and open symbols, respectively) at 77 K for (A) TiO_2 hp (squares), POM/hp–EtOH (circles) and POM/hp (triangles) and (B) POM/P25–HCl (squares) and POM/P25 (circles).

broad absorption band, ascribed to the charge transfer process from O^{2-} to Ti^{4+} responsible for the band-gap. TiO_2 is an indirect semiconductor [27] and the band-gap energies of the samples, estimated from the tangent lines in the plots of the modified Kubelka–Munk function, $[F(R'_\infty)h\nu]^{1/2}$ versus the energy of exciting light [28], give rise to band-gap values ranging between 3.0 and 3.2 eV. It can be observed a slight decrease of reflectance (i.e. increase of absorbance) in the visible region by adding the POM to both commercial and home prepared bare TiO_2 samples. Moreover a slight bathochromic shift of the charge transfer process O^{2-} to Ti^{4+} is observed for the samples containing the POM species on the TiO_2 surface with respect to the correspondent bare TiO_2, ascribed to some modification in the coordination environment of TiO_2.

Fig. 4 shows the Raman spectra of both bare TiO_2 Degussa P25 and home prepared samples along with selected POM supported samples prepared in the presence of HCl or EtOH during the

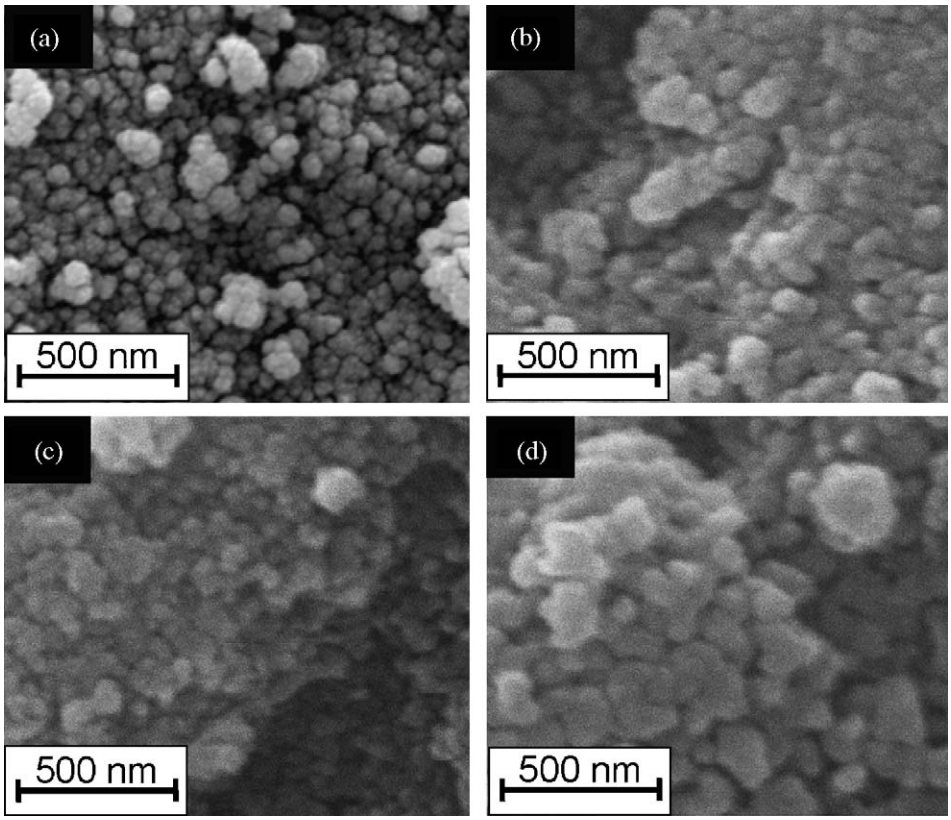

Fig. 2. SEM micrographs of: (a) bare TiO_2 hp, (b) POM/hp, (c) POM/hp–EtOH and (d) POM/hp–HCl.

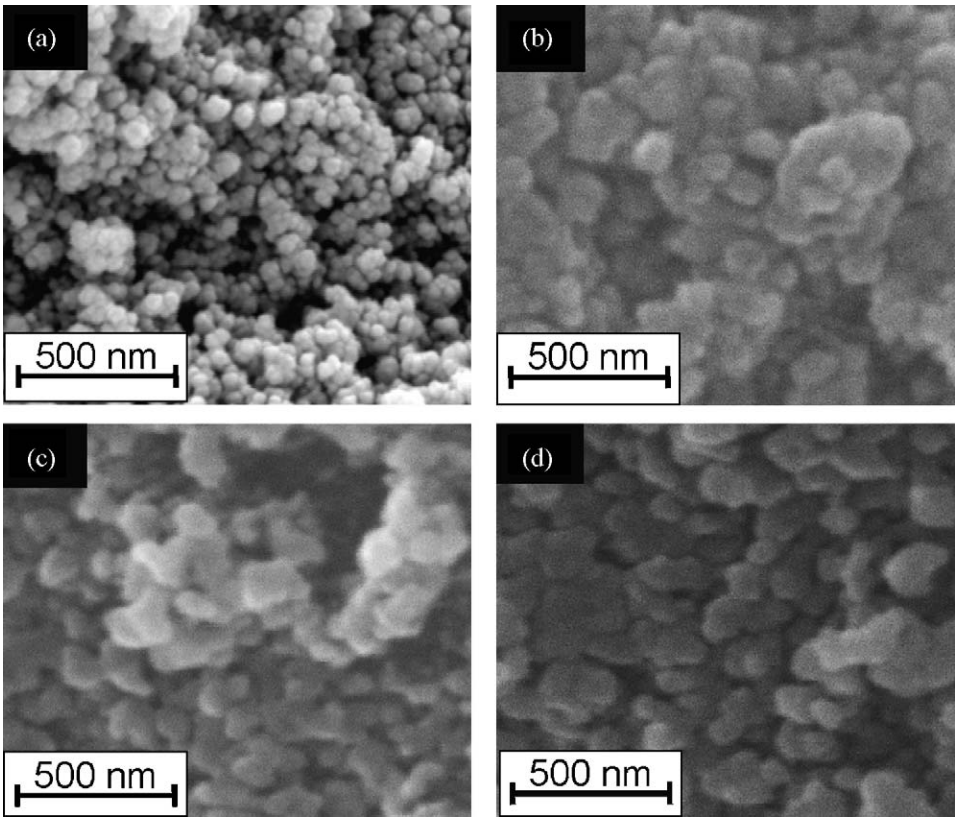

Fig. 3. SEM micrographs of: (a) bare TiO_2 Degussa P25, (b) POM/P25, (c) POM/P25–EtOH and (d) POM/P25–HCl.

impregnation step. Both spectra of the bare TiO_2 samples show the characteristic bands corresponding to anatase crystalline phase. In the bare TiO_2 Degussa P25, Raman bands at 395, 516 and 637 cm^{-1}, assigned to modes of TiO_2 anatase, are clearly observed [29]. In the spectra of bare TiO_2 hp peaks attributed to the rutile phase are also present and they are located at 444 and at 609 cm^{-1} (shoulder) [29]. Intense peaks at 142 and 144 cm^{-1}, assigned to rutile and anatase, respectively, are out of the range of the spectra reported in Fig. 4. In the POM supported samples, the four POM characteristic bands are also present, i.e. a sharp and intense band at 1006 cm^{-1} and a peak at 990 cm^{-1}, assigned to P–O vibrations and bands at lower wavenumbers, attributed to W–O (983 cm^{-1}) and W–O–W (903 cm^{-1}) vibrations [13,30]. The sharper and more intense band at 1006 cm^{-1} is present for all of the loaded samples and no significant shift can be observed. After impregnation of the POM onto the TiO_2, the Raman peaks corresponding to P–O and W–O vibration modes were broadened with respect to the bare POM spectrum, and consequently the resolution between these peaks decreases. At the same time the peak intensity corresponding to the W–O–W vibration became relatively weaker. These findings can be attributed to a H-bonding interaction between the oxygen atom of the Keggin anion and the hydroxyl groups on the TiO_2 surface, as observed before [4,31].

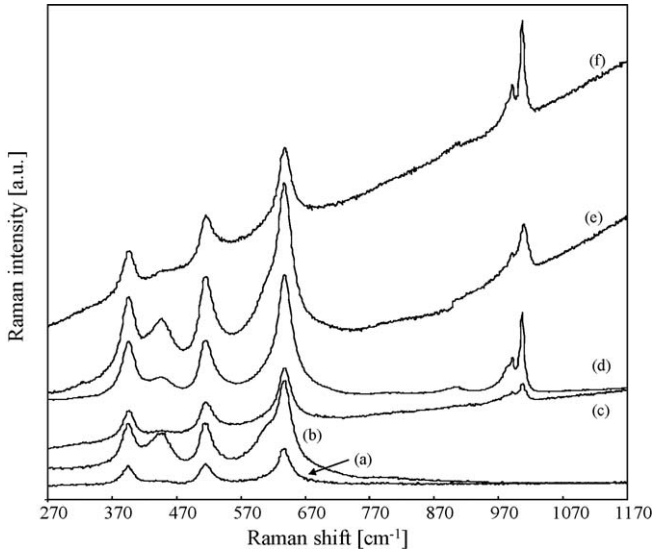

Fig. 4. Raman spectra of: (a) bare TiO_2 Degussa P25, (b) bare TiO_2 hp, (c) POM/P25–HCl, (d) POM/hp–HCl, (e) POM/hp–EtOH and (f) POM/P25–EtOH.

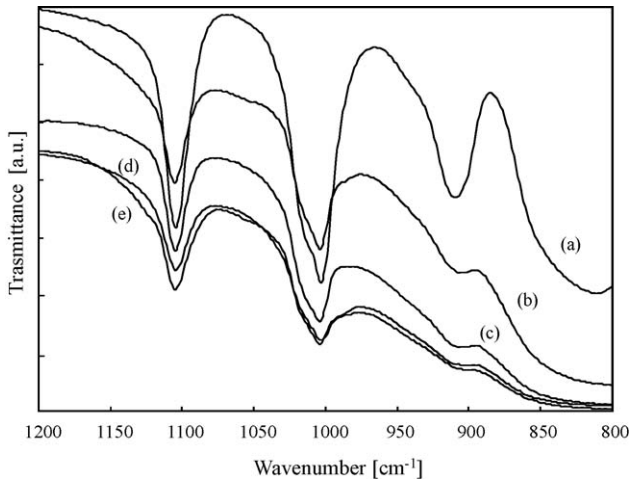

Fig. 5. FT-IR spectra of KBr pellets of: (a) commercial $H_3PW_{12}O_{40}$, (b) POM/P25, (c) POM/hp–EtOH, (d) POM/hp and (e) POM/hp–HCl.

The solid samples were also analyzed by FTIR in order to confirm the structural integrity of the Keggin unit on the TiO_2 surface. The structure of the $PW_{12}O_{40}^{3-}$ anion consists of a PO_4 tetrahedron surrounded by four W_3O_9 groups formed by edge sharing octhaedra. These groups are connected each other by corners sharing oxygen atoms [32]. This arrangement gives rise to four types of stretching bands between 1100 and 700 cm^{-1}, the fingerprint region for this kind of compounds. The presence of the TiO_2 cut-off at wavenumbers lower than 900 cm^{-1} does not allow to clearly notice part of these range. Fig. 5 shows the FTIR spectra of the POM loaded TiO_2 samples along with the bare POM. It is clear that the four main stretching vibrations of the skeletal bonds in PW_{12} are located at ca. the same wavenumbers when the POM is loaded on the surface of both commercial and home prepared TiO_2, indicating that the Keggin geometry of PW_{12} was still preserved in the binary material. The typical band for P–O absorption (1080 cm^{-1}) is displayed, along with the W=O stretching (990 cm^{-1}). The two peaks at ca. 910 and 810 cm^{-1} [33], attributed to two types of W–O–W units are partially covered by the cut-off of the titanium dioxide.

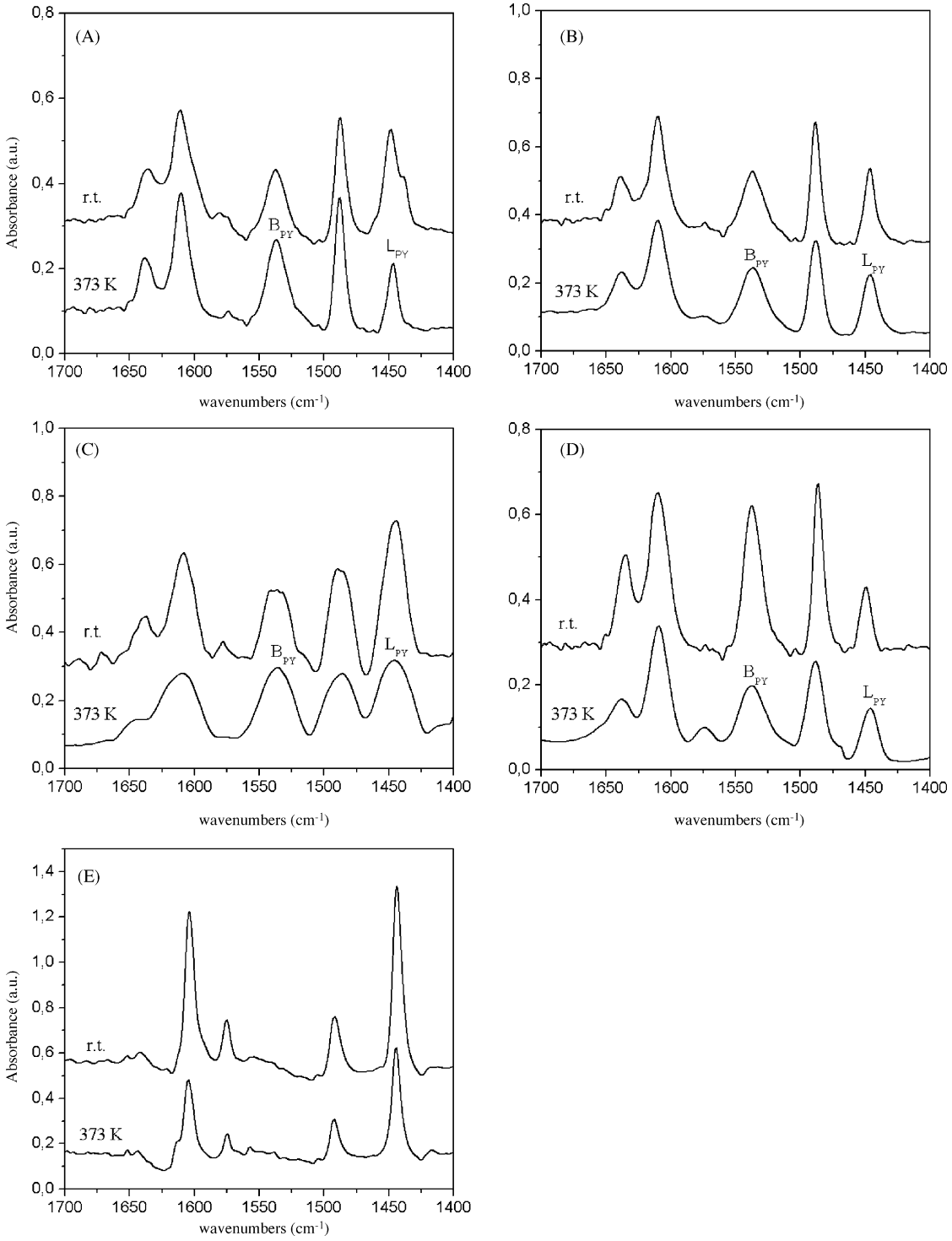

Fig. 6. FT-IR spectra of pyridine adsorbed at room temperature and outgassed at 373 K over samples: (a) POM/P25, (b) POM/P25–HCl, (c) POM/hp, (d) POM/hp–EtOH and (e) TiO_2 hp.

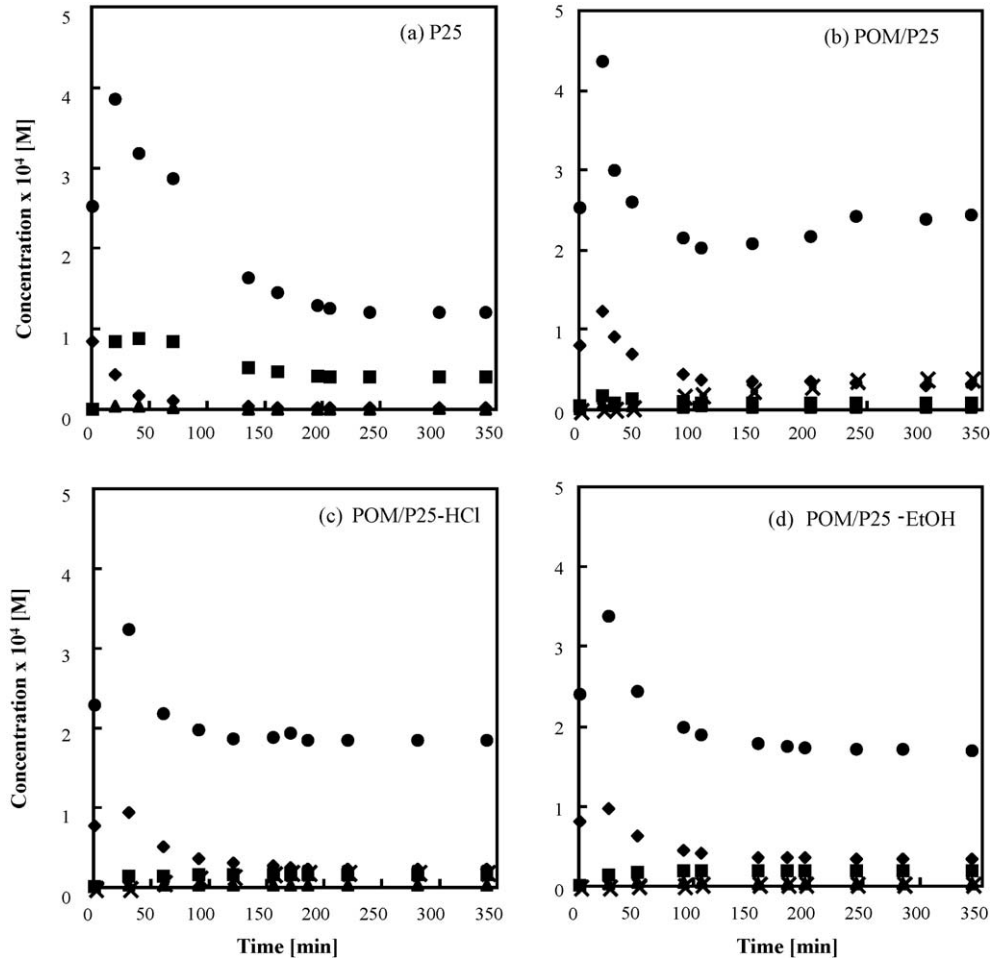

Fig. 7. Evolution of 2-propanol (◆), propanone (■), propene (×), acetaldehyde (▲) concentrations and total organic carbon amount (●) versus irradiation time for reaction in the gas–solid system in the presence of: (a) TiO_2 Degussa P25, (b) POM/P25, (c) POM/P25–HCl and (d) POM/P25–EtOH.

The bands attributed to the Keggin's unit skeletal vibrations did not become more intense in the samples where the POM was supported on the TiO_2 with respect to those attributed to the bare POM, as expected in the absence of anion–anion interactions [33,13]. This insight could be attributed to the interactions between the Keggin units and the surface of the TiO_2 support, considering the relative low amount of POM and its homogeneous dispersion onto the support surface. H-bonding interactions cannot be excluded, considering the broadening of the bands indicating that the vibrations are disturbed by dipole–dipole interactions [13], probably between the Keggin units and the TiO_2 surface, confirming the Raman results.

The FT-IR spectra recorded upon adsorption of pyridine (Py) over TiO_2 hp and selected POM/TiO_2 samples, recorded at room temperature and outgassed at 373 K, are reported in Fig. 6. In the case of the bare support, bands at 1604, 1574, 1491 and 1444 cm^{-1} are registered, which correspond to the 8a, 8b, 19a and 19b vibration modes of Py coordinated to Lewis-type acid sites, respectively [34]. After Py adsorption, samples loaded with tungstophosphoric acid show bands at ca. 1610, 1575, 1490 and 1447 cm^{-1}, assigned to 8a, 8b, 19a and 19b vibration modes, respectively, of Py coordinated to Lewis-type acid sites. Along with these bands, another one at 1538 cm^{-1}, which corresponds to vibration mode 19b of protonated pyridine, is also registered. In order to establish a sequence in the Brönsted acidity of these samples the Brönsted Py/Lewis Py (BPy/LPy) ratio has been calculated by rationing the area measured for the peak ascribed to the 19b vibration of the pyridinium ion by the area ascribed to the 19b vibration mode of the coordinated pyridine in the spectra registered on the samples after outgassing at 373 K, shown in Fig. 6. The Brönsted acid sites with respect to the Lewis ones are ca. double for all of the POM loaded samples. In particular the (BPy/LPy) ratio are in the range 1.98–2.35. It is worth noting that these values are maximum, 2.35 and 2.24, for the samples where the POM was impregnated in water solution onto the P25 and the TiO_2 hp samples, respectively. Table 1 shows the (BPy/LPy) ratio for some representative binary materials.

3.2. Photoreactivity experiments

Blank reactivity tests were performed under the same experimental conditions used for the photoreactivity experiments but in the absence of catalyst, oxygen or light. No reactivity was observed in all these cases, so it was concluded that the simultaneous presence of O_2, catalyst, and irradiation is needed for the occurrence of the 2-propanol degradation process. The photoreactivity runs started when the system achieved the steady-state condition in the dark, that was reached, due to the strong adsorption showed by the solid samples, after 4 h of fluxing the reactive mixture into the photoreactor.

Figs. 7 and 8 report the values of the outlet 2-propanol concentration versus irradiation time for runs carried out by using both bare TiO_2 and POM impregnated TiO_2 powders as the photomediators.

In Fig. 7, reporting the photocatalytic activity of P25 based samples, the initial increase of 2-propanol concentration during

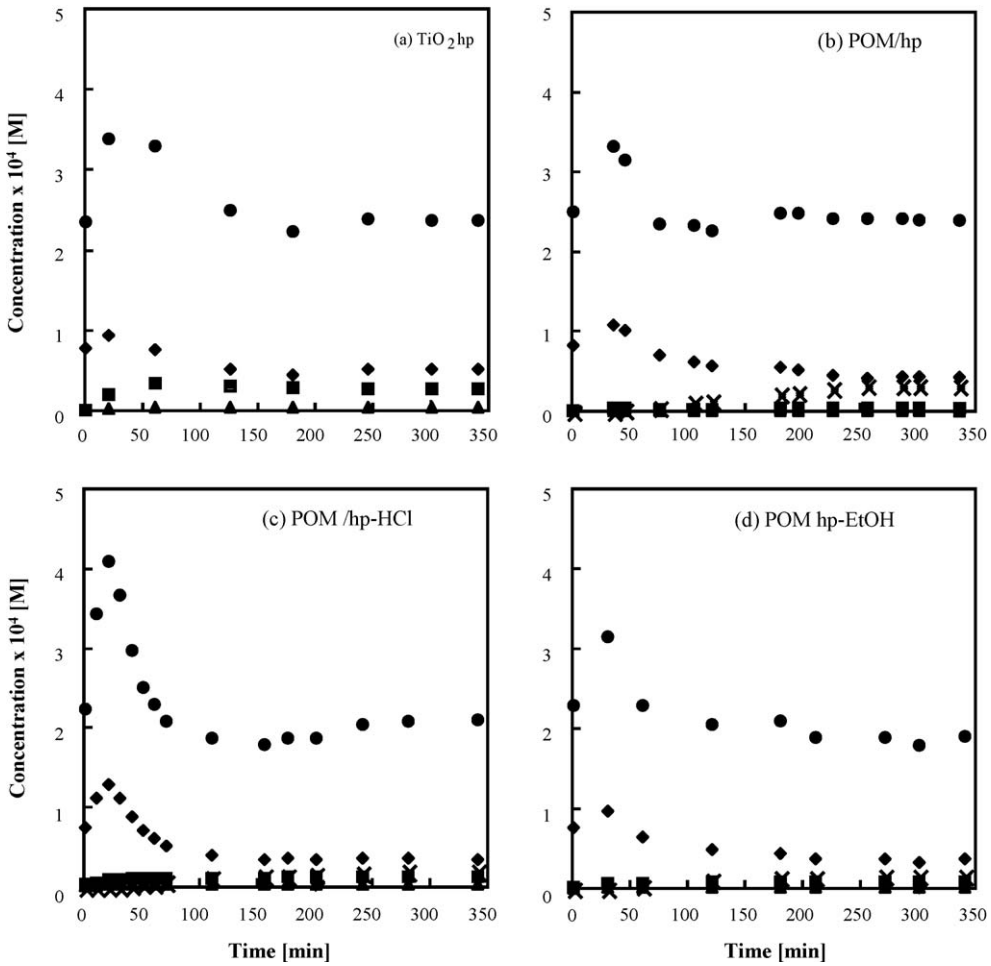

Fig. 8. Evolution of 2-propanol (◆), propanone (■), propene (×), acetaldehyde (▲) concentrations and total organic carbon amount (●) versus irradiation time for reaction in the gas–solid system in the presence of: (a) TiO_2 hp, (b) POM/hp, (c) POM/hp–HCl and (d) POM/hp–EtOH.

the first 30 min of irradiation can be attributed to the photo/thermo desorption of the substrate that was adsorbed during the stabilization period under dark conditions. This effect is evident in the POM supported samples but not in the run carried out with bare P25. Fig. 8, reporting the photocatalytic activity of TiO_2 hp based samples, shows the photo/thermo desorption of the substrate in all the four runs. A successive decrease in the concentration of 2-propanol was observed in any case.

2-Propanol completely disappeared in the course of the photocatalytic reaction only in the presence of TiO_2 Degussa P25, as reported in Fig. 7(a). During the course of all runs the decrease of the substrate concentration is observed along with a simultaneous formation of propanone and/or propene. In the particular case of either commercial or home prepared bare TiO_2 samples, propanone was the main product formed. On the other hand, propene formation was observed as an intermediate product exclusively in the runs where POM was present. In any case the concentration of the intermediate products reached at steady-state conditions depended on the photocatalyst used. Acetaldehyde and isopropylether were also revealed as minor products during the course of all the runs along with traces of mesityl oxide and isobuthyl-methyl-ketone, detected also as gaseous products. Moreover, under the current experimental conditions, carbon dioxide was also generated and analyzed by gas chromatography. The total concentration of organic carbon is also depicted in Figs. 7 and 8, showing in some cases a loss essentially due to the

Table 2
Reactivity results for 2-propanol disappearance. The values reported[a] correspond to initial reaction rate (r), the percentage of conversion (X), and selectivity in the intermediates and the final product (CO_2).

	r (mol/s)	X	Selectivity (%)				
			Propanone	Propene	Acetaldehyde	Isopropylether	CO_2
POM/P25	2.5×10^{-8}	63	14	80	2	4	0
POM/P25–HCl	2.7×10^{-8}	71	28	38	3	3	27
POM/P25–EtOH	2.3×10^{-8}	58	39	9	3	1	47
POM/hp	2.0×10^{-8}	49	7	82	2	8	0
POM/hp–HCl	2.0×10^{-8}	54	32	43	3	7	15
POM/hp–EtOH	1.9×10^{-8}	51	20	40	3	6	31
Degussa P25	4.1×10^{-8}	99	47	0	1	0	52
TiO_2 hp	1.4×10^{-8}	37	90	0	8	0	0

[a] The reported values are the average of three measurements.

formation of CO_2. In particular, an important loss in the organic carbon atom concentration for the run carried out with Degussa P25 can be observed in Fig. 7(a). This loss corresponds to the amount revealed as CO_2 in the gas phase. Table 2 reports the 2-propanol disappearance rate, its conversion, yield in propanone, propene, acetaldehyde and isopropylether for all the runs, indicating quantitatively the behaviour of the runs depicted in Figs. 7 and 8.

The 2-propanol disappearance rate ($r_{2\text{-prop}}$) was calculated by applying the following mass balance equation on the whole continuous photoreactor:

$$r_{2\text{-prop}} = W(C^0_{2\text{-prop}} - C_{2\text{-prop}}) \quad (1)$$

in which W is the volumetric gas flow rate and $C^0_{2\text{-prop}}$ and $C_{2\text{-prop}}$, the inlet and outlet 2-propanol molar concentrations, respectively.

The perusal of Table 2 indicates that the reaction rate of bare TiO_2 Degussa P25 sample for 2-propanol degradation was the highest one, and the value obtained by using the home prepared TiO_2 was ca. one third. The three POM supported on Degussa P25 samples showed a similar photoactivity, that was lower than that observed for the bare Degussa P25. On the contrary, the activity of the POM supported samples based on TiO_2 hp increased on respect to the bare home prepared one. Conversion of 2-propanol, calculated after 5 h of reaction (i.e. at steady-state conditions), was almost complete or ca. half by using bare P25 or hp, respectively. The conversion of 2-propanol increased for the POM supported on TiO_2 hp samples, and decreased for those supported on P25 with respect to the corresponding bare samples. It is worth noting that between the POM supported samples the conversion was slightly higher for the samples prepared in HCl medium.

The perusal of the results reveals that the presence of the POM onto the TiO_2 surface strongly influenced the photocatalytic behaviour of the TiO_2 bare samples as far as the selectivity in the intermediate products is concerned. Indeed, due to the increased surface acidity, the selectivity of the POM–TiO_2 binary catalysts versus the propene formation increased whereas versus propanone it drastically decreased. No propene was revealed for the bare TiO_2 samples.

The presence of ethanol or HCl during the impregnation step of the POM onto the TiO_2 surface did not influence qualitatively the behaviour of the loaded photocatalyst as far as selectivity to the intermediate products is concerned, in comparison with the results obtained with the solids impregnated by using POM water solution. However, it is worth noting that in the last case the selectivity towards propanone decreased and that versus propene increased, both for P25 and hp based samples (see Table 2). The selectivity to acetaldehyde was nearly the same for all of the POM containing samples, although bare TiO_2 hp showed the highest selectivity (8%) among all of the samples.

Isopropylether was found exclusively during the runs carried out by using the POM supported samples.

As far as mineralization to CO_2 is concerned, it reached the value of ca. 50% when Degussa P25 was used, whereas it was negligible by using the bare hp. The presence of different solvents (ethanol, HCl or H_2O) during the POM impregnation step seems to influence the mineralization ability of the resulting samples. In particular, both P25 and hp POM loaded photocatalysts prepared in the presence of water, were not able to mineralize 2-propanol, while when EtOH or HCl were present during the impregnation step, the obtained samples were able only to partially mineralize the substrate and the amount of produced CO_2 was always smaller than that obtained in the presence of the bare P25. Anyway, it is interesting to note that samples POM/hp–HCl and, particularly, POM/hp–EtOH showed a remarkable increase in their mineralization ability with respect to the bare TiO_2 hp.

In order to study the influence of the presence of water vapour (3.4×10^{-4} M) on the photoreactivity, some experiments were carried out in the absence of water vapor, concluding that the presence of water, in the experimental conditions used was indifferent, as far as reaction rate, conversion and yield in intermediates are concerned. This finding can be explained by considering the formation of water as a reaction product [16–22]. The presence of water is necessary in order to displace propanone from the surface [35] and we hence conclude that the amount of water produced during the reaction is enough to allow the restoration of the active sites. The behaviour of 2-propanol contrasts with that observed with some probe aromatic molecules such as toluene [36,37], where a strong deactivation occurred in the absence of water vapor in the gas–solid system by using TiO_2 Degussa P25, due to the strong interaction of benzoate species produced onto the surface sites.

It is generally proposed that propene formation involved either surface Brönsted or Lewis acid sites, leading to hydrogen bonded or coordinated 2-propanol species, respectively [38,39].

3.3. Mechanistic aspects

The photo-oxidation runs indicated that 2-propanol degradation occurred via the formation of various intermediates. As mentioned before, the main intermediates derived from 2-propanol photo-oxidation in gas–solid regime by using bare TiO_2 were propanone and acetaldehyde. The same compounds were observed by Bickley et al. [18] under similar conditions. There is a general agreement in the literature that the main products of 2-propanol photocatalytic oxidation in a gas–solid system by using bare TiO_2 are propanone, CO_2 and H_2O, with selectivity versus propanone or CO_2 depending strongly on the experimental conditions [16–19]. Moreover, isopropyl ether [23] or propene [16] were also found. FTIR spectroscopy allowed to observe, besides propanone, also propene [16], mesityl oxide [40] and ethanoic acid [16] adsorbed on the catalyst surface. Some species can strongly interact at the surface thus blocking the active sites [16].

It is generally accepted that $^{\bullet}OH$ radicals generated on the surface of the photocatalyst as shown in Eqs. (2)–(4), act as the primary oxidant species. The hydroxyl radicals are produced in the following reactions:

$$TiO_2 + h\nu \rightarrow TiO_2\,(e^-_{cb}, h^+_{vb}) \quad (2)$$

$$OH^-_{(surf)} + h^+_{vb} \rightarrow {}^{\bullet}OH_{(surf)} \quad (3)$$

$$H_2O_{(ads)} + h^+_{vb} \rightarrow {}^{\bullet}OH_{(surf)} + H^+ \quad (4)$$

$$O_{2(ads)} + e^- \rightarrow O^-_{2(ads)} \quad (5)$$

The reaction between $^{\bullet}OH$ radicals and 2-propanol gives rise to the formation of propanone and acetaldehyde. Ohko et al. [20] report that the generated $^{\bullet}OH$ radical reacts with 2-propanol, abstracting a hydrogen atom to form a radical, that subsequently, reacts with another hydroxyl radical forming propanone:

$$(CH_3)_2CHOH + {}^{\bullet}OH \rightarrow (CH_3)_2C^{\bullet}OH + H_2O \quad (6)$$

$$(CH_3)_2C^{\bullet}OH + {}^{\bullet}OH \rightarrow (CH_3)_2CO + H_2O \quad (7)$$

Analogously, the formation of propanoate radical, obtained according to reaction (8), that can react with a $^{\bullet}OH$ radical to evolve into acetaldehyde and methanol (9), could be hypothesized.

$$(CH_3)_2CHOH + {}^{\bullet}OH \rightarrow (CH_3)_2CHO^{\bullet} + H_2O \quad (8)$$

$$(CH_3)_2CHO^{\bullet} + {}^{\bullet}OH \rightarrow CH_3CHO + CH_3OH \quad (9)$$

Acetaldehyde was found in the reaction system in much lower concentration than propanone, indicating that reactions (8) and (9) represent a less significant side effect. The presence of methanol was not confirmed in the reacting system probably because it was immediately decomposed to CO_2.

It is important to stress that although POM could generate $^{\bullet}OH$ radicals under UV radiation, this event depends on the type of POM and on the incident irradiation wavelength in order to promote an electron from the highest occupied molecular orbital (HOMO) to the lowest unoccupied molecular orbital (LUMO). For instance, Hiskia et al. [5] reported that for the Keggin type POM ($PW_{12}O_{40}^{3-}$), used in our work, the minimum energy allowing this transition corresponds to 270 nm. Due to the fact that our lamp do not emits energy at this wavelength, we can exclude the formation of $^{\bullet}OH$ radicals on the POM surface.

Moreover, propene was found in the photocatalytic degradation of 2-propanol when the binary material POM–TiO_2 was used as the photocatalyst. This finding is attributed to the strong acidic character of the binary POM–TiO_2 loaded samples. This result suggests the occurrence of an alternative photo-degradation pathway to those already mentioned above. The propene molecule could derive from the dehydration of the adsorbed 2-propanol on an appropriate acidic surface site. A thermally activated mechanism for the dehydration reaction where strong acid sites and weak basic sites are involved is suggested in the literature [39]. Probably the UV light is able to supply the energy that in the catalytic reaction is provided by heating the system. The formation of isopropyl ether can be explained by considering a reaction that involves an intermolecular dehydration of two 2-propanol molecules. This reaction has been suggested to occur involving both acid and basic sites on the solid depending on the number of acid sites instead of on their strength [39]. The E1 mechanism requires only very strong acid sites, responsible for the formation of the olefin, whereas the E2 mechanism, involving both the acid and the basic sites, leads also to the formation of ether.

4. Conclusions

The photocatalytic degradation of 2-propanol occurred successfully in gas–solid regime by using commercial and home prepared TiO_2 impregnated with $H_3PW_{12}O_{40}$. Propanone and propene were the main intermediate products while acetaldehyde and isopropylether showed to be the minor intermediates. Carbon dioxide and water were the main oxidation products. Home prepared TiO_2, obtained by hydrolysis of $TiCl_4$, consisted of incompletely crystallized anatase and rutile particles and the impregnation with $H_3PW_{12}O_{40}$ produced samples where POM resulted well dispersed onto the surface of TiO_2 and where, as indicated by the vibrational spectroscopies, the Keggin geometry of the PW_{12} was still preserved and the POM units were anchored onto the TiO_2 surface by means of H-bonding. Photoreactivity experiments showed that 2-propanol degradation rate by using commercial TiO_2 Degussa P25 was 2.4 faster than that using TiO_2 hp. The activity of TiO_2 hp was enhanced by the impregnation with the POM, whereas it was depleted for TiO_2 Degussa P25. The selectivity to the intermediate products changed dramatically between POM containing samples and bare TiO_2. By using both the bare TiO_2 samples, the main intermediate product was propanone, whereas when the binary material POM/TiO_2 was used, propene was found as the main intermediate product. The different selectivity can be ascribed to differences in the physico-chemical characteristics of the solid surface. The selectivity to propene detected over the POM/TiO_2 samples is in good agreement with the Brönsted to Lewis ratio measured from the pyridine adsorption FT-IR spectra.

Acknowledgements

The authors wish to thank MIUR (Rome) and Università degli Studi di Palermo for financial support.

References

[1] A. Fujishima, K. Hashimoto, T. Watanabe, TiO_2 Photocatalysis: Fundamentals and Applications, Bkc, Tokyo, 1999.
[2] S. Yanagida, A. Nakajima, T. Sasaki, Y. Kameshima, K. Okada, Chem. Mater. 20 (2008) 3757.
[3] X. Qu, Y. Guo, C. Hu, J. Mol. Catal. A: Chem. 262 (2007) 128.
[4] Y. Guo, C. Hu, J. Mol. Catal. A: Chem. 262 (2007) 136.
[5] A. Hiskia, A. Mylonas, E. Papaconstantinou, Chem. Soc. Rev. 30 (2001) 62.
[6] E. Papaconstantinou, Chem. Soc. Rev. 18 (1989) 1.
[7] P. Kormali, A. Troupis, T. Triantis, A. Hiskia, E. Papaconstantinou, Catal. Today 124 (2007) 149.
[8] I.V. Kozhevnikov, Chem. Rev. 98 (1998) 171.
[9] A.P. Alivisatos, Science 271 (1996) 933.
[10] N. Mizuno, M. Misono, Chem. Rev. 98 (1998) 199.
[11] M.J. Verhoet, P. Kooyman, J.A. Peters, H. van Bekkum, Micropor. Mesopor. Mater. 27 (1999) 365.
[12] A.L. Villa, P.B. Sels, D.E. De Vos, P.A. Jacobs, J. Organ. Chem. 64 (1999) 7267.
[13] E. Fontananova, L. Donato, E. Drioli, L.C. López, P. Favia, R. D'Agostino, Chem. Mater. 18 (2006) 1561.
[14] U. Lavrenčič Štangar, N. Grošelj, B. Orel, Ph. Colomban, Chem. Mater. 12 (2000) 3745.
[15] T. Tachikawa, M. Fujitsuka, T. Majima, J. Phys. Chem. C 111 (2007) 5259.
[16] M. Fernández-García, A. Martínez-Arias, J.C. Hanson, J.A. Rodríguez, Chem. Rev. 104 (2004) 4063.
[17] M. Addamo, M. Del Arco, M. Bellardita, D. Carriazo, A. Di Paola, E. García-López, G. Marcì, C. Martín, L. Palmisano, V. Rives, Res. Chem. Intermed. 33 (2007) 465.
[18] R.I. Bickley, G. Munuera, F.S. Stone, J. Catal. 31 (1973) 398.
[19] S.A. Larson, J.A. Widengree, J. Falconer, J. Catal. 157 (1995) 611.
[20] Y. Ohko, K. Hashimoto, A. Fujishima, J. Phys. Chem. A 101 (1997) 8057.
[21] F. Arsac, D. Bianchi, J.M. Chovelon, C. Ferronato, J.M. Herrmann, J. Phys. Chem. A 110 (2006), 4202 and 4213.
[22] E. Ortiz-Islas, T. López, J. Navarrete, X. Bokhimi, R. Gómez, J. Mol. Catal. A: Chem. 228 (2005) 345.
[23] (a) J.E. Rekoske, M.A. Barteau, J. Catal. 165 (1997) 57;
(b) M. Ponzi, C. Duschatzly, A. Carrascull, E. Ponzi, Appl. Catal. A 169 (1998) 373;
(c) D. Haffad, A. Chambellan, J.C. Lavalley, J. Mol. Catal. A 168 (2001) 153.
[24] A. Gervasini, A. Auroux, J. Catal. 131 (1991) 190.
[25] V. Rives, C. Martín, A. Montero, Spanish Patent 200,100,688 (2001).
[26] Y. Hu, H.L. Tsai, C.L. Huang, Mater. Res. Eng. A 344 (2003) 209.
[27] F.P. Koffyberg, K. Dwight, A. Wold, Solid State Commun. 30 (1979) 433.
[28] Y.I. Kim, S.J. Atherton, E.S. Brigham, T.E. Mallouk, J. Phys. Chem. 97 (1993) 11802.
[29] G.A. Trompsett, G.A. Bowmaker, R.P. Cooney, J.B. Metson, K.A. Seatkins, J. Raman Spectrosc. 26 (1995) 57.
[30] U.B. Mioč, R.Z. Dimitrijević, M. Davidović, Z.P. Nedić, M.M. Mitrović, Ph. Colomban, J. Mater. Sci. 29 (1994) 3705.
[31] U. Lavrenčič Štangar, B. Orel, A. Régis, Ph. Colomban, J. Sol Gel Sci. Technol. 8 (1997) 965.
[32] M.T. Pope, Heteropoly and Isopolyoxometalates, Springer–Verlag, New York, 1983.
[33] C. Rocchiccioli-Deltcheff, M. Fournier, R. Franck, R. Thouvenot, Inorg. Chem. 22 (1983) 207.
[34] E.P. Parry, J. Catal. 2 (1963) 371.
[35] G. Munuera, F.S. Stone, Disc. Faraday Soc. 52 (1971) 205.
[36] G. Marcì, M. Addamo, V. Augugliaro, S. Coluccia, E. García-López, V. Loddo, G. Martra, L. Palmisano, M. Schiavello, J. Photochem. Photobiol. A: Chem. 160 (2003) 105.
[37] G. Martra, V. Augugliaro, S. Coluccia, E. García-López, V. Loddo, L. Marchese, L. Palmisano, M. Schiavello, Stud. Surf. Sci. Catal. 130 (2000) 665.
[38] A. Gervasini, Y. Fenyvesi, A. Auroux, Catal. Lett. 43 (1997) 219.
[39] M.E. Manríquez, T. López, R. Gómez, J. Navarrete, J. Mol. Catal. A 220 (2004) 229.
[40] W. Xu, D. Raftery, J.S. Francisco, J. Phys. Chem. 107 (2003) 4537.